2013 IEEE/RSJ International Conference on
Intelligent Robots and Systems (IROS)
November 3-7, 2013. Tokyo, Japan

A Compliant Humanoid Walking Strategy Based on the Switching of State Feedback Gravity Compensation Controllers

Emmanouil Spyrakos-Papastavridis, Gustavo A. Medrano-Cerda,

Nikos G. Tsagarakis, Jian S. Dai and Darwin G. Caldwell

***Abstract*—This paper provides stability analyses for two different types of desired gravity compensation controllers, employing both motor and link feedback, and describes a means by which these controllers can be used to control a compliant humanoid robot in order to ensure the successful execution of walking trajectories. Given the challenging task of controlling compliant bipedal systems, owing to their possession of under-actuated degrees of freedom, the full actuator and link dynamics are accounted for. The proposed walking strategy involves a process of switching between three distinct controllers which is contingent upon the force feedback provided by the force/torque sensors embedded in the robot's feet. These controllers were tuned using a simulation model of the robot and were then implemented on the compliant COMAN legs, whose performance of walking confirms the controllers' stability, in addition to the walking scheme's efficacy.**

I. INTRODUCTION

HUMANOID robot walking has long been considered an exciting research challenge due mainly to the intricacy associated with bipedal dynamics and hence with the pertinent control algorithms. One of the most famous walking bipeds is perhaps the ASIMO, that was capable of performing walking trajectories [1] using a posture control algorithm, which was a combination of various schemes, such as ground reaction force control, online modification of the ZMP and foot landing position control. In addition, an intuitive control strategy was propounded in [2], wherein the authors suggested five criteria to be satisfied in order to guarantee a biped's successful execution of a trajectory. A sensory reflex control method was presented in [3], whereby the robot was stabilized during a desired trajectory by performing online modification of its posture, its foot positioning, as well as of the trajectory itself. More recently, bipedal walking was achieved through the utilization of a linear inverted pendulum model upon which a force controller was designed [4].

Additionally, when dealing with compliant humanoids, the devise of more involved control techniques is inevitable owing to the increase in the complexity of the dynamics. Even though simpler motor PID schemes may provide tracking on stiff humanoids, this might not necessarily be the case for compliant humanoids. On the one hand, using single pendulum models to develop tracking controllers [4] leads to a reduction in the tuning complexity, although it may not provide a viable solution for compliant bipeds as there is no accounting for the entirety of the states [5]. Contrarily, using full-body dynamics can be computationally demanding and difficult to implement [5], especially when dealing with compliant systems. Therefore, the method described in this paper may be viewed as a compromise between the previously described techniques, since it offers a higher degree of modeling accuracy as compared to the inverted pendulum approach, while at the same time reduces the complexity associated with full-body dynamics.

However, despite the afore-stated disadvantage of this class of bipedal systems, their inherent compliance tends to enhance their stabilization capability and thus there is currently a trend of shifting towards flexible machines. [6] describes the use of a dynamic, real-time trajectory that allowed the COmpliant huMANoid (COMAN) [7] to perform walking. Moreover, [8] reports on a technique of merging the inverted pendulum model with a compliant Cartesian model used to predict the center-of-mass (COM) position and then employing Internal Model Control (IMC) to achieve the required tracking performance. The method was validated experimentally on the COMAN. [9] outlines the development of a compliant humanoid walking strategy using a combination of a posture-based state machine and a tendon-driven compliant actuator torque control scheme to guarantee trajectory tracking.

Gravity compensation control has been the topic of several works. [10] proposed a PD plus gravity compensation controller that has been mathematically proven to asymptotically stabilize robots composed of elastic joints. In [11], there is a description of the derivation of strict Lyapunov functions based on the energy shaping principle, which are then used to demonstrate global asymptotic stability. The approach involving the employment of full-state feedback controllers on flexible joint robots has been treated in [12]. On the other hand, [13] presented a PD plus on-line gravity compensation controller for a flexible joint that has been validated through both analytical and experimental results. This paper expands on the afore-mentioned works by means of providing stability proofs for equal-actuated and over-actuated gravity compensation

E. Spyrakos-Papastavridis, G. A. Medrano-Cerda, N. G. Tsagarakis and D. G. Caldwell are with the Department of Advanced Robotics, Istituto Italiano di Tecnologia, via Morego, 30, 16163 Genova {emmanouil.spyrakos, gustavo.cerda, nikos.tsagarakis, darwin.caldwell} at iit.it

Jian S. Dai is with the Centre for Robotics Research, King's College London, Strand, London, WC2R 2LS, England, United Kingdom {jian.dai} at kcl.ac.uk

The work is supported by the EU Project AMARSI.

controllers employing both motor and link feedback. Full-body gravity compensation control of humanoids was initially presented in [14] and proved to be an apt choice as far as the execution of dynamical tasks was concerned. [15] on the other hand proposes the use of virtual gravity compensation torque control for the development of a balance controller capable of attaining natural bipedal walking. [16] describes a method by which the ground reaction forces could be translated into joint torques, while mathematically proving this specific controller's passivity. Additionally, the topic of semi-passive walking through the control of a compliant ankle joint has been reported in [17], while [18] describes the exploitation of the robot's passive compliance for the construction of semi-passive motion primitives.

The method proposed in this paper involves the use of PDD control (motor position, motor velocity and link velocity) on 6 degree-of-freedom (DOF) single support and 3-DOF double support models of the robot, in combination with gravity compensation control. The dynamical models include the full actuator dynamics, i.e. the motor and link dynamics appearing before and after the elastic element. Furthermore, the joint controllers are based purely on position control, while a state machine is used to switch between the three distinct models as well as between the three different gravity vectors, in accordance with the force/torque sensor feedback.

The rest of the paper is structured as follows; section II introduces the dynamical models, section III describes the PDD plus gravity compensation control schemes and their associated theoretical stability proofs, as well as the switching mechanism. Additionally, the simulation, controller tuning and experimental results are seen in section IV, while section V addresses the conclusions and future work.

II. DYNAMICAL MODEL

A. Compliant Robot Dynamics

This section describes the dynamics of both the single and double support phases of a humanoid robot with compliant drives. For the single support case, we consider a generic n-degree of freedom robot with n drives, one for each degree of freedom. The robot and motor dynamics are described by the following two equations:

$$M_J(q)\ddot{q} + N\dot{q} + C(q,\dot{q})\dot{q} + Pq - P\theta = \tau_g(q) \tag{1}$$

$$J\ddot{\theta} + D\dot{\theta} - Pq + P\theta = V_{TG}V_m \tag{2}$$

where q and θ denote the link and motor positions, while $M_J(q)$, N and $C(q,\dot{q}) \in R^{n\times n}$ are the inertia, damping and Coriolis/centripetal matrices respectively, $\tau_g(q)$ is the gravity torque vector, $V_{TG} \in R^{n\times n}$ is the voltage-to-torque gain matrix and V_m represents the motor voltages. $P \in R^{n\times n}$ is a diagonal matrix with positive entries representing the passive spring stiffness between the motors and the robot links, while $J, D \in R^{n\times n}$ are the motor inertia and damping.

For the double support case, we consider a generic j-degree of freedom robot with n_i-drives for each degree of freedom $i = 1,2 \dots j$. The total number of drives is $n = \sum_{i=1}^{j} n_i$. The dynamics may be described as follows [19]:

$$M_{J0}(q)\ddot{q} + N_0\dot{q} + C_0(q,\dot{q})\dot{q} + S_m^T P(S_m q - \theta) = \tau_{g0}(q) \tag{3}$$

$$J\ddot{\theta} + D\dot{\theta} - PS_m q + P\theta = V_{TG}V_m \tag{4}$$

where $M_{J0}(q)$, N_0, $C_0(q,\dot{q}) \in R^{j\times j}$ are this phase's counterparts of $M_J(q)$, N and $C(q,\dot{q})$ while $S_m^T \in R^{j\times n}$ is a matrix composed of ones and zeros, with its columns associated to the system's motors and its rows to the system's joints. Arranging the motor equation so that the first n_1 drives are connected to link 1, the next n_2 are connected to link 2 and so on, then S_m^T is given as:

$$S_m^T = \begin{bmatrix} \underbrace{1\,1\cdots 1}_{n_1} & 0 & \cdots & 0 \\ 0 & \underbrace{1\,1\cdots 1}_{n_2} & \cdots & 0 \\ \vdots & \vdots & \ddots & \vdots \\ 0 & 0 & \cdots & \underbrace{1\,1\cdots 1}_{n_j} \end{bmatrix} \tag{5}$$

B. Single and Double Support Models

In order to maintain an adequate degree of accuracy when mathematically describing the robot, it was essential to include all the sagittal joints in the system's model. This could be seen as an improvement when compared to employing an inverted pendulum model, while it also dispenses with the need for full-body dynamics. 6-DOF models (Fig. 1) were used to represent the single support phases, while a 3-DOF model (Fig. 1) was employed for the modeling of the double support phase. Fig. 1 also depicts the left and right ground reaction forces (GRF) F_{Z_L} and F_{Z_R}. The gravity vectors differed significantly between the single and double support phases and hence had to be computed independently. The entries of the 6-DOF single support vectors were arranged as follows:

$$\tau_g = [\tau_{sa} \quad \tau_{sk} \quad \tau_{sh} \quad \tau_{swh} \quad \tau_{swk} \quad \tau_{swa}]^T$$

with $\tau_{sa}, \tau_{sk}, \tau_{sh}, \tau_{swh}, \tau_{swk}, \tau_{swa}$ being the support ankle, knee and hip, and swing hip, knee and ankle torques respectively. On the other hand, the elements of the 3-DOF double support vector were ordered as follows:

$$\tau_{g0} = [\tau_a \quad \tau_k \quad \tau_h]^T$$

with τ_a, τ_k, τ_h representing the ankle, knee and hip torques respectively. An important property of the gravity vector is the following:

$$\left\| \frac{\partial \tau_g(q)}{\partial q} \right\| = \left\| \frac{\partial^2 U_g(q)}{\partial q^2} \right\| \le \alpha \tag{6}$$

for some $\alpha > 0$; here $U_g(q)$ denotes the potential energy due to gravity, and $\tau_g(q) = -\left(\partial U_g(q)/\partial q\right)^T$. A similar expression holds for the double support model gravity vector $\tau_{g0}(q)$.
Three dynamical models were used in total to model the various phases of the walking trajectory.
Table I summarizes the above models with LSS, RSS and DS standing for 'left single support', 'right single support', and 'double support' respectively. This approach resulted in the attainment of a set of mathematical models that provided a closer approximation to the non-linear nature of the robot's dynamics when switching between the various phases of a walking trajectory, as opposed to using a single model during the whole trajectory.

TABLE I
DYNAMICAL MODELS

Model	DOF's
DS	3
LSS	6
RSS	6

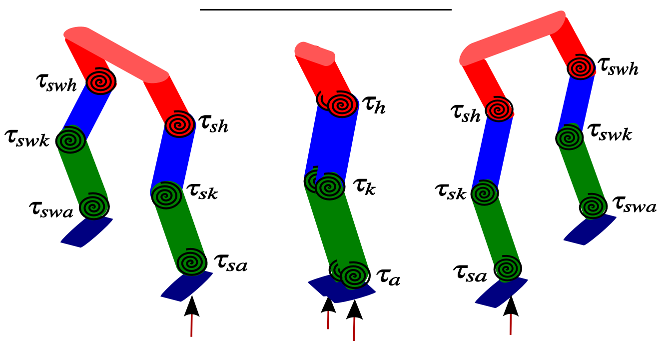

Figure 1. Left single support (left), double support (center) and right single support (right) models.

III. CONTROL STRATEGY

A. PDD Control plus Gravity Compensation

1. Single Support Controller

The control law for system $(1)-(2)$ is given by:

$$V_m = K_{m1}(q_d - \theta) - K_{m2}\dot{\theta} - K_{j2}\dot{q} + u_{gc} \tag{7}$$

where u_{gc} is the gravity compensation term and q_d is the desired position, while K_{m1}, K_{m2} and K_{j2} are the diagonal, positive definite motor position, motor velocity and link velocity feedback gain matrices.
For the single support u_{gc} is given by:

$$u_{gc} = -V_{TG}^{-1} \cdot (V_{TG}K_{m1}P^{-1} + I) \cdot \tau_g(q) \tag{8}$$

The matrix:

$$T_S = \begin{bmatrix} P & -P \\ -P & V_{TG}K_{m1} + P \end{bmatrix} \tag{9}$$

is defined separately for use in the subsequent section. Moreover, θ_d is defined as:

$$\theta_d = q_d - P^{-1}\tau_g(q_d) \tag{10}$$

since we used a desired gravity compensation scheme.

2. Double Support Controller

The control law in this case may be represented as follows:

$$V_m = K_{m1}(S_m q_d - \theta) - K_{m2}\dot{\theta} - K_{j2}\dot{q} + u_{gc} \tag{11}$$

For the double support u_{gc} is given by:

$$u_{gc} = -V_{TG}^{-1}(V_{TG}K_{m1}P^{-1} + I)(S_m^T)^+\tau_{g0}(q) \tag{12}$$

where $(S_m^T)^+$ denotes the Moore-Penrose pseudoinverse of S_m^T. Then T_D is defined as:

$$T_D = \begin{bmatrix} S_m^T P S_m & -S_m^T P \\ -P S_m & V_{TG}K_{m1} + P \end{bmatrix} \tag{13}$$

Additionally, for the double support:

$$\theta_d = S_m q_d - P^{-1}(S_m^T)^+\tau_{g0}(q_d) \tag{14}$$

We also define the matrices:

$$\gamma = N \cdot (D + V_{TG}K_{m2}) - \frac{(V_{TG}K_{j2})^2}{4} \tag{15}$$

$$\gamma_0 = N_0 \cdot (D + V_{TG}K_{m2}) - \frac{(V_{TG}K_{j2})^2}{4} \tag{16}$$

B. Proof of Closed-Loop Stability

1. Single Support Controller

Theorem 1: If $\lambda_{min}(T_S) > \alpha$ and $\lambda_{min}(\gamma) > 0$ when $q = q_d$ in (12), then there is a unique equilibrium solution $[q_d^T \quad \theta_d^T \quad 0 \quad 0]^T$, that is globally asymptotically stable.

Proof 1: Setting $q = q_d$ in (8) gives rise to a desired link position gravity compensation controller. Using (1), (2), (7), (8), (10) and setting zero velocities and accelerations, gives the following expression (after some algebraic manipulations):

$$T_S \begin{bmatrix} q - q_d \\ \theta - \theta_d \end{bmatrix} = \begin{bmatrix} \tau_g(q) - \tau_g(q_d) \\ 0 \end{bmatrix} \tag{17}$$

Letting $x = [q^T \quad \theta^T]^T$, $H(x) = x_d + T_S^{-1}\tau(x)$

where $\tau(x) = \begin{bmatrix} \tau_g(q) - \tau_g(q_d) \\ 0 \end{bmatrix}$, the contraction mapping theorem [20] yields:

$$\|H(x) - H(y)\| \leq \lambda_{max}\left(T_S^{-1}\right)\alpha\|x - y\|$$

$$\therefore \qquad \|H(x) - H(y)\| \leq \frac{\alpha}{\lambda_{min}(T_S)}\|x - y\|$$

$\frac{\alpha}{\lambda_{min}(T_S)} < 1$ is a sufficient condition to ensure that (17) has a unique solution. Hence, this gives:

$$\lambda_{min}(T_S) > \alpha \tag{18}$$

A crucial step in the construction of a suitable Lyapunov function is the selection of an appropriate auxiliary function. We therefore propound the following, that can be seen to differ from similar functions presented in [10], [13]:

$$W(q,\theta) = \frac{1}{2} q_E^T T_S q_E + U_g(q) - U_g(q_d) + q_E^T \begin{bmatrix} \tau_g(q_d) \\ 0 \end{bmatrix} \tag{19}$$

, where $q_F = \begin{bmatrix} q \\ \theta \end{bmatrix}$, $q_{F_d} = \begin{bmatrix} q_d \\ \theta_d \end{bmatrix}$, $q_E = (q_F - q_{F_d})$.

It can be demonstrated that (19) has a unique minimum at the equilibrium point (q_d, θ_d), through the following equation:

$$\nabla W(q,\theta) = T_S q_E + \begin{bmatrix} \tau_g(q_d) - \tau_g(q) \\ 0 \end{bmatrix} = 0 \tag{20}$$

From (18) we can conclude that the Hessian is positive definite and hence (19) has a unique minimum at (q_d, θ_d):

$$\nabla^2 W(q_d, \theta_d) = T_S - \begin{bmatrix} \frac{\partial \tau_g(q)}{\partial q} & 0 \\ 0 & 0 \end{bmatrix} > 0 \tag{21}$$

The following Lyapunov function formulation is therefore permitted:

$$V(q,\theta) = \frac{1}{2} \dot{q}_F^T M(q) \dot{q}_F + W(q,\theta) \geq 0 \tag{22}$$

where $M = \begin{bmatrix} M_J & 0 \\ 0 & J \end{bmatrix}$.

Obtaining the time derivative of the above function yields:

$$\dot{V}(q,\theta) = \dot{q}_F^T M(q) \ddot{q}_F + \tfrac{1}{2} \dot{q}_F^T \dot{M}(q) \dot{q}_F - \dot{q}_F^T \begin{bmatrix} \tau_g(q) - \tau_g(q_d) \\ 0 \end{bmatrix} + \dot{q}_F^T T_S q_E$$

$$\dot{V}(q,\theta) = \dot{q}_F^T \begin{pmatrix} \begin{bmatrix} -C & 0 \\ 0 & 0 \end{bmatrix} \dot{q}_F + \frac{1}{2} \dot{M}(q) \dot{q}_F \\ + \begin{bmatrix} \tau_g(q_d) - \tau_g(q) \\ 0 \end{bmatrix} - T_S q_E \\ - \begin{bmatrix} N & 0 \\ V_{TG} K_{j2} & D + V_{TG} K_{m2} \end{bmatrix} \dot{q}_F \end{pmatrix} + \dot{q}_F^T T_S q_E$$

$$+ \dot{q}_F^T \begin{bmatrix} \tau_g(q) - \tau_g(q_d) \\ 0 \end{bmatrix}$$

$$\dot{V}(q,\theta) = -\dot{q}_F^T \begin{bmatrix} N & 0 \\ V_{TG} K_{j2} & D + V_{TG} K_{m2} \end{bmatrix} \dot{q}_F \leq 0 \tag{23}$$

Since the matrix in (23) is not symmetric, proving its positive definiteness requires the performance of certain manipulations, commencing with a more succinct representation for brevity:

$$\begin{bmatrix} X & 0 \\ Y & Z \end{bmatrix} > 0 \tag{24}$$

An equivalent condition to (24) is

$$\begin{bmatrix} \frac{X + X^T}{2} & \frac{Y^T}{2} \\ \frac{Y}{2} & \frac{Z + Z^T}{2} \end{bmatrix} > 0 \tag{25}$$

Computing the Schur complement of (25) [21] and taking into account that X, Y and Z are diagonal matrices, we have:

$$X \cdot Z - \frac{Y^2}{4} > 0 \tag{26}$$

Finally, setting $X = N$, $Z = D + V_{TG} K_{m2}$, $Y = V_{TG} K_{j2}$ and since all these matrices are diagonal we arrive at equation (15) and the condition $\lambda_{min}(\gamma) > 0$.

It may now be observed that $\dot{V} = 0$ if and only if $\dot{q}_F = 0$. By then substituting $\ddot{q}_F = \dot{q}_F = 0$ into the closed-loop equations (1), (2) and (7), we obtain:

$$P(q - \theta) = \tau_g(q) \tag{27}$$

$$P(\theta - q) = V_{TG}\big(K_{m1}(q_d - \theta) + u_{gc}\big) \tag{28}$$

By carrying out algebraic manipulations, it may be seen that (27) and (28) are equivalent to (17), that was previously shown to possess the unique equilibrium solution $[q_d^T \quad \theta_d^T \quad 0 \quad 0]^T$. Thus, it can be concluded that this is also the largest invariant subset among the set of states yielding $\dot{q}_F = 0$, in which case invocation of La Salle's theorem leads to the conclusion that the desired equilibrium point is globally asymptotically stable.

2. Double Support Controller

Theorem 2: If $\lambda_{min}(T_D) > \alpha$ and $\lambda_{min}(\gamma_0) > 0$ when $q = q_d$ in (12), then there is a unique equilibrium solution $[q_d^T \quad \theta_d^T \quad 0 \quad 0]^T$, that is globally asymptotically stable.

Proof 2: Setting $q = q_d$ in (12), using (3), (4), (11), (12), (14) and setting zero velocities and accelerations, gives the following expression (after some algebraic manipulations):

$$T_D \begin{bmatrix} q - q_d \\ \theta - \theta_d \end{bmatrix} = \begin{bmatrix} \tau_{g0}(q) - \tau_{g0}(q_d) \\ 0 \end{bmatrix} \tag{29}$$

which possesses a unique solution if $\lambda_{min}(T_D) > \alpha$.

The auxiliary function for this case would be the same as (19), with the only difference being the replacement of T_S with T_D. The performance of calculations identical to those presented earlier, allows us to arrive at (23). Hence, the resulting Lyapunov function is similar to the one derived for the single support controller, although the matrices are of different dimensions. Setting $\ddot{q}_F = \dot{q}_F = 0$ in (3), (4) and (11), we acquire the following equations:

$$S_m^T P_m S_m q - S_m^T P_m \theta = \tau_g(q) \tag{30}$$

$$P_m \theta - P_m S_m q = V_{TG}\big(K_{m1} S_m (q_d - \theta) + u_{gc}\big) \tag{31}$$

Following a similar approach to that used in Proof 1 and invoking LaSalle's theorem, allows us to conclude that the desired equilibrium point is globally asymptotically stable.

C. *Phase Switching*

The procedure entailing the switching between the various phases of the trajectory and thus between the various sets of gains, was based upon a finite state machine (FSM) that catered for both the single and double support phases, as demonstrated by Fig. 2.

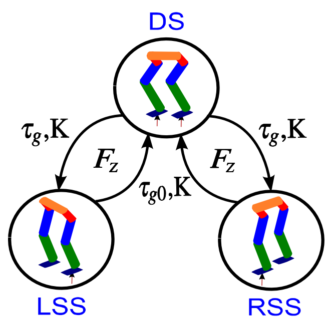

Figure 2. Walking controller finite state machine.

A preview control approach [4] was employed for the generation of the trajectory, which was computed in an offline manner. Contrarily, the joint control and gravity compensation strategies were formulated online in relation to the position/velocity and force/torque feedback respectively, as is portrayed in Fig. 3.

The gravity compensation value was altered not only when a phase switch was detected but also as new reference positions were fed to the controller by the trajectory generator. Therefore, equations (8) and (12) allowed for the modification of the gravity compensation voltages in accordance with the robot's configuration. The gravity vector varied during all state transitions, as did the PDD gains. The switching of the gains was contingent upon the force feedback values provided by the force/torque sensors at the robot's feet. There was a need for the definition of certain conditions, that when satisfied, would trigger the gain switching action at each phase.

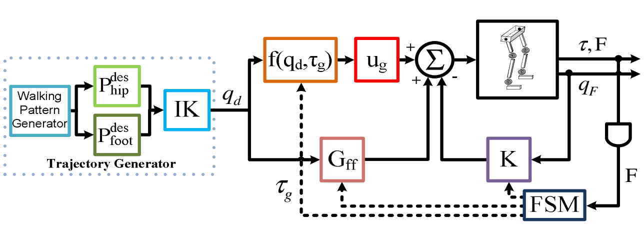

Figure 3. Walking strategy control loop block diagram.

These conditions were based upon our knowledge of the robot's mass and ground reaction forces, that allowed us to derive a condition for switching from double to single support when a certain force limit was exceeded on either one of the feet. On the other hand, the transition from single to double support gains occurred when neither of the normal forces exceeded the predefined limits.

IV. Controller Tuning and Experiments

A. *Simulation and Controller Design*

The simulation procedure involved the use of a series of dynamical models (Table I) of the robot with each one containing a complete representation of the actuator dynamics. Hence, three different controllers were designed for the DS, RSS and LSS models. Notice that the LSS model is in essence a mirror-image of the RSS model and thus the mere rearrangement of the latter's gain matrices was sufficient for the construction of the former's gain matrices.

It was crucial that the controller would be capable of displaying a satisfactory degree of tracking in the simulation, as this could indicate its potential tracking of walking trajectories when implemented on the robot. Fig. 4 depicts the support and swing legs' simulated tracking of the walking trajectory.

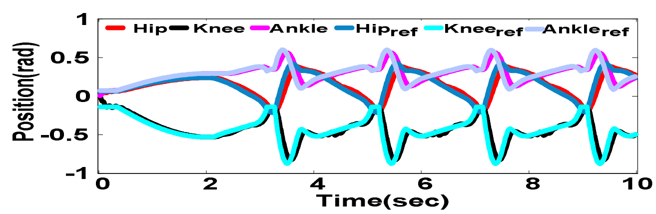

Figure 4. Walking trajectory tracking in simulation.

B. *Experimental Validation*

In terms of specifications, the COMAN's lower body is comprised of 15 DOFs, with a height and weight of 79 cm and 17.65 kg respectively. Each sagittal compliant joint incorporates three position sensors (2 absolute and 1 relative) and a torque sensor, in addition to 6-axis force/torque sensors at the ankles.

The described controllers were implemented on the humanoid, while the control scheme of Fig. 3 was used to ensure tracking of the desired walking trajectory. The step length during walking was 12 cm and the trajectory was generated at a frequency of approximately 0.8 Hz. Explicit details regarding the trajectory generation framework may be found in [22][23].

In order to assess the robot's overall stability, an inspection of the joint tracking and Cartesian CoM position during the trajectory was required, as portrayed by Figs. 5 and 6. It is evident from these plots that the ankle demonstrates the poorest tracking capability of all the joints and this could be owed to the fact that it has been assigned the cumbersome task of supporting the mass of the whole robot. Furthermore, the left and right foot and center of mass positions depicted in Fig. 6 were computed using the link position data rather than the motor position data, thus accounting for the robot's oscillatory behavior during motion due to the passive joint elasticity. Given the link COMs, the use of forward kinematics (FK) enabled the calculation of the Cartesian COM trajectory [23].

A challenging aspect of the control strategy was related to the tuning of the switching conditions which demanded a relatively high degree of precision. These conditions were predominantly concerned with the contact force magnitudes on both feet as mentioned earlier. An imprecise switching command would mean that the model used at a given instant would not provide an accurate description of the system's current state. This in turn would imply the use of an incorrect set of gains providing an input that would either over-compensate or under-compensate for the system's dynamics. Therefore, the selection of the parameter values was based upon our knowledge of the GRFs exerted on each of the models being used. Fig. 7 portrays the GRFs measured on the right foot during walking, with the light purple, red and yellow areas representing the double support, right single support and left single support respectively.

Additionally, Fig. 8 displays the various joint control signal values produced during walking.

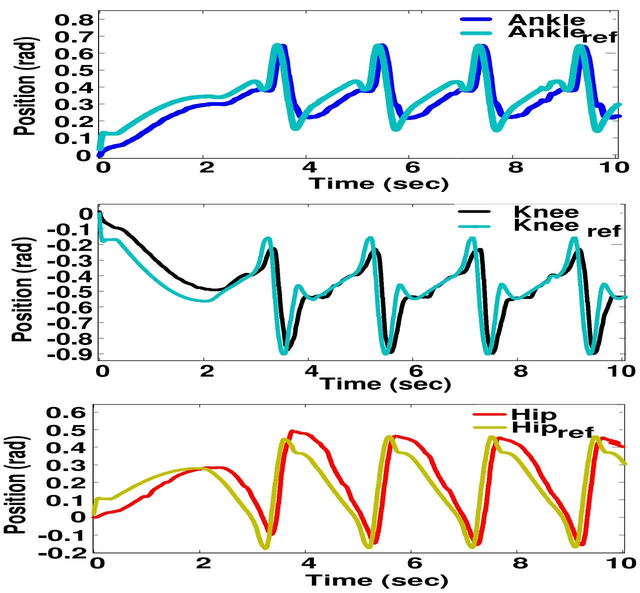

Figure 5. Ankle, knee and hip joint tracking.

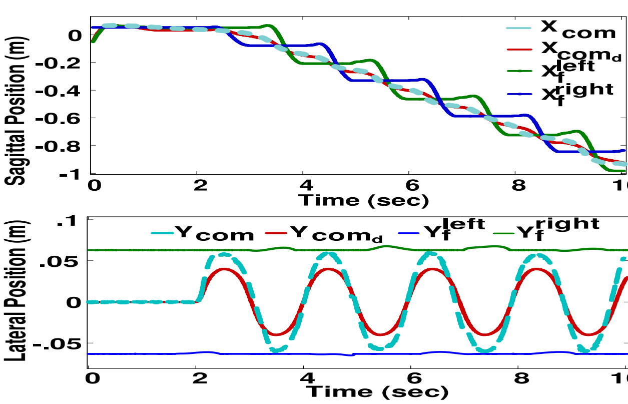

Figure 6. Cartesian X and Y CoM positions during walking.

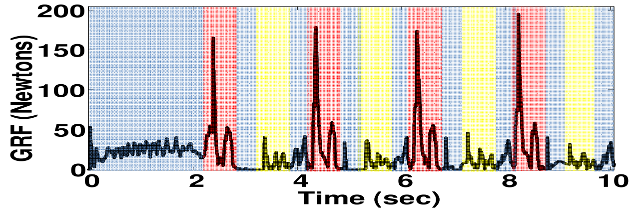

Figure 7. Right foot ground reaction forces during walking.

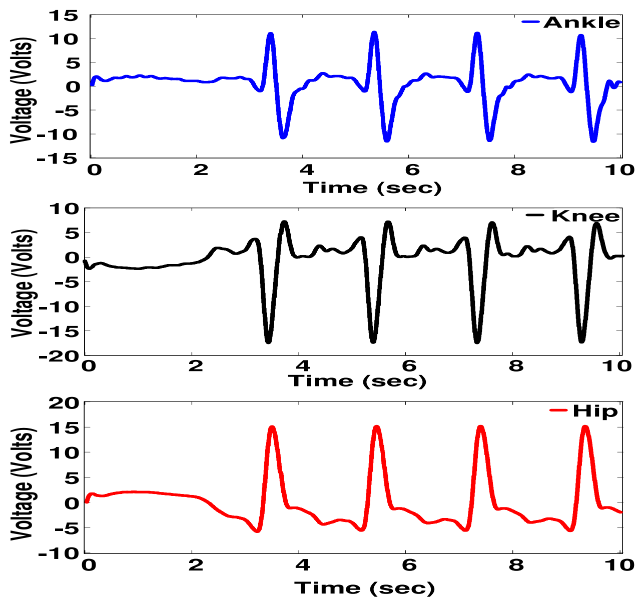

Figure 8. Ankle, knee and hip control voltages during walking.

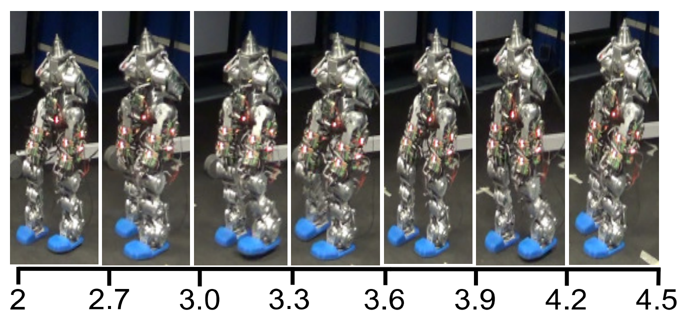

Figure 9. COMAN snapshots during walking.

C. Controller Specifications

Despite presenting the theory behind the controller's stability in III.C, it must now be proven that our designed controllers satisfy not only conditions $\lambda_{min}(T_S) > \alpha$ and $\lambda_{min}(\gamma) > 0$, but also conditions $\lambda_{min}(T_D) > \alpha$ and $\lambda_{min}(\gamma_0) > 0$. From a theoretical point of view, the stability analyses allow us to conclude global stabilization for each distinct model, using our proposed controller. In practice however, such an assumption might not always be valid and could only be verified numerically. Thus, we will focus on obtaining a bound for the gravity vector derivative, represented by the constant α in (6). Table II lists the $\lambda_{min}(T_D)$, $\lambda_{min}(T_S)$, $\lambda_{min}(\gamma_0)$ and $\lambda_{min}(\gamma)$ values.

The table below indicates that the stability criteria are satisfied by all three controllers.

TABLE II
STABILITY CRITERIA

Controller	α	$\lambda_{min}(T_D)$	$\lambda_{min}(\gamma_0)$	$\lambda_{min}(T_S)$	$\lambda_{min}(\gamma)$
DS	68.0360	128.400	1.0540	-	-
LSS, RSS	51.2735	-	-	74.6880	0.5931

V. CONCLUSION

A PDD control scheme combined with gravity compensation allowed for the development of a strategy that permitted COMAN to successfully execute walking trajectories. Three different dynamical models were utilized for the description of the various phases of the walking trajectory, resulting in three sets of gains. The control scheme employed motor position, motor velocity and link velocity feedback, in addition to force feedback, that enabled switching between the various gain matrices and gravity vectors using an FSM. Moreover, each distinct controller's stability was mathematically proven through the establishment of two conditions that were both shown to be satisfied by all three controllers. The experimental results allow us to deduce that the proposed approach can successfully track a desired dynamic walking trajectory on a compliant humanoid robot. Furthermore, this method not only enhances the mathematical accuracy when compared to the inverted pendulum model but it also reduces the complexity and computational burden of implementing full-body dynamics.

ACKNOWLEDGMENT

This work is supported by the ICT - 248311 – AMARSI European Commission project.

REFERENCES

[1] K. Hirai, M. Hirose, Y. Haikawa and T. Takenaka, "The development of Honda humanoid robot," *Proc. IEEE Int. Conf. on Robotics and Automation, vol. 2, pp. 1321-1326, 1998.*

[2] J. Pratt and G. Pratt, "Intuitive control of a planar bipedal walking robot," *Proc. IEEE Int. Conf. on Robotics and Automation, vol. 3, pp. 2014-2021, 1998.*

[3] Q. Huang and Y. Nakamura, "Sensory reflex control for humanoid walking," *IEEE Transactions on Robotics, vol. 21, pp. 977-984, 2005.*

[4] S. Kajita, M. Morisawa, K. Miura, S. Nakaoka, K. Harada, K. Kaneko, F. Kanehiro and K. Yokoi, "Biped walking stabilization based on linear inverted pendulum tracking," *Proc. IEEE/RSJ Int. Conf. on Intelligent Robots and Systems, pp. 4489-4496, 2006.*

[5] N. Sugimoto and J. Morimoto, "Switching Multiple LQG Controllers Based on Bellman's Optimality Principle: Using Full-State Feedback to Control a Humanoid Robot," *Proc. IEEE/RSJ Int. Conf. on Intelligent Robots and Systems, pp. 3185-3191, 2011.*

[6] B. Ugurlu, N. G. Tsagarakis, E. Spyrakos-Papastavridis and D. G. Caldwell, "Compliant joint modification and real-time dynamic walking implementation on bipedal robot ccub," *Proc. IEEE Int. Conf. on Mechatronics, pp. 833-838, 2011.*

[7] N. G. Tsagarakis, S. Morfey, G. A. Medrano-Cerda, Z. Li and D. G. Caldwell, "Compliant Humanoid COMAN: Optimal Joint Stiffness Tuning for Modal Frequency Control," *Proc. IEEE Int. Conf. on Robotics and Automation, 2013.*

[8] L. Colasanto, N. G. Tsagarakis, Z. Li and D. G. Caldwell, "Internal Model Control for Improving the Gait Tracking of a Compliant Humanoid Robot," *Proc. IEEE/RSJ Int. Conf. on Intelligent Robots and Systems, pp. 5347-5352, 2012.*

[9] B. Lim, M. Lee, J. Kim, J. Lee, J. Park, K. Seo and K. Roh, "Control design to achieve dynamic walking on a bipedal robot with compliance," *Proc. IEEE Int. Conf. on Robotics and Automation, pp. 79-84, 2012.*

[10] P. Tomei, "A Simple PD Controller for Robots with Elastic Joints," *IEEE Transactions on Automatic Control, vol. 36, pp. 1208-1213 1991.*

[11] R. Kelly and V. Santibánez, "Global Regulation of Elastic Joint Robots Based on Energy Shaping," *IEEE Transactions on Automatic Control, vol. 43, pp. 1451-1456, 1998.*

[12] A. Albu-Schäffer and G. Hirzinger, "State feedback controller for flexible joint robots: A globally stable approach implemented on DLR's light-weight robots," *Advanced Robotics, vol. 15, pp. 799-814, 2001.*

[13] A. De Luca, B. Siciliano and L. Zollo, "PD Control with on-line gravity compensation for robots with elastic joints: Theory and Experiments," *Automatica, vol. 41, pp. 1809-1819, 2005.*

[14] S. Hyon and G.Cheng, "Passivity-Based Full-Body Force Control for Humanoids and Application to Dynamic Balancing and Locomotion," *Proc. IEEE/RSJ Int. Conf. on Intelligent Robots and Systems, pp. 4915-4922, 2006.*

[15] K. Seo, J. Kim and K. Roh, "Towards natural bipedal walking: Virtual gravity compensation and capture point control," *Proc. IEEE/RSJ Int. Conf. on Intelligent Robots and Systems, pp. 4019-4026, 2012.*

[16] O. Ly, M. Lapeyre and P. Oudeyer, "Bio-Inspired vertebral column, compliance and semi-passive dynamics in a lightweight humanoid robot," *Proc. IEEE/RSJ Int. Conf. on Intelligent Robots and Systems, pp. 1465-1472, 2011.*

[17] S. Hyon, J. G. Hale and G. Cheng, "Full-Body Compliant Human-Humanoid Interaction: Balancing in the Presence of Unknown External Forces," *IEEE Transactions on Robotics, vol. 23, pp. 884-898, 2007.*

[18] A. Omer, R. Ghorbani, H. Lim and A. Takanishi, "Semi-passive dynamic walking for humanoid robot using controllable spring stiffness on the ankle joint," *Proc. IEEE/ASME Int. Conf. on Autonomous Robots and Agents, pp. 1600-1605, 2009.*

[19] E. Spyrakos-Papastavridis, G. Medrano-Cerda, N. G. Tsagarakis, J. S. Dai and D. G. Caldwell, "Gravity Compensation Control of Compliant Joint Systems with Multiple Drives," *Proc. IEEE Int. Conf. on Robotics and Automation, 2013.*

[20] H. K. Khalil, "Nonlinear Systems," *Third Edition, Prentice Hall,2002.*

[21] S. Skogestad, I. Postlethwaite, "Multivariable Feedback Control: Analysis and Design," *Second Edition, John Wiley & Sons, 2001.*

[22] Z. Li, N. G. Tsagarakis, D. G. Caldwell, "Walking Trajectory Generation for Humanoid Robots with Compliant Joints: Experimentation with COMAN Humanoid," *Proc. IEEE Int. Conf. on Robotics and Automation, pp. 836-841, 2012.*

[23] Z. Li, N. G. Tsagarakis, D. G. Caldwell, "Walking pattern generation for a humanoid robot with compliant joints," *Autonomous Robots, vol. 35, pp. 1-14.*